How to cite: *Angew. Chem. Int. Ed.* **2023**, *62*, e202303570
doi.org/10.1002/anie.202303570

Photothermal Therapy **Hot Paper**

Multi-Channel Lanthanide Nanocomposites for Customized Synergistic Treatment of Orthotopic Multi-Tumor Cases

Yuxin Liu, Xingjun Zhu, Zheng Wei, Kefan Wu, Junfang Zhang, Francesco G. Mutti, Hong Zhang, Felix F. Loeffler,* and Jing Zhou**

Abstract: Simultaneous photothermal ablation of multiple tumors is limited by unpredictable photo-induced apoptosis, caused by individual intratumoral differences. Here, a multi-channel lanthanide nanocomposite was used to achieve tailored synergistic treatment of multiple subcutaneous orthotopic tumors under non-uniform whole-body infrared irradiation prescription. The nanocomposite reduces intratumoral glutathione by simultaneously activating the fluorescence and photothermal channels. The fluorescence provides individual information on different tumors, allowing customized prescriptions to be made. This enables optimal induction of hyperthermia and dosage of chemo drugs, to ensure treatment efficacy, while avoiding overtherapy. With an accessional therapeutic laser system, customized synergistic treatment of subcutaneous orthotopic cancer cases with multiple tumors is possible with both high efficacy and minimized side effects.

[*] Y. Liu, Dr. J. Zhang, Dr. F. F. Loeffler
Department of Biomolecular Systems, Max Planck Institute of Colloids and Interfaces
14476 Potsdam (Germany)
E-mail: Felix.Loeffler@mpikg.mpg.de

Y. Liu, Z. Wei, Prof. Dr. J. Zhou
Beijing Key Laboratory for Optical Materials and Photonic Devices, Capital Normal University
Beijing 100048 (China)
E-mail: jingzhou@cnu.edu.cn

Y. Liu, Z. Wei, K. Wu, Prof. Dr. F. G. Mutti, Prof. Dr. H. Zhang
Van′ t Hoff Institute for Molecular Sciences, Molecular Photonics & HIMS-Biocat University of Amsterdam
1098 XH Amsterdam (The Netherlands)
E-mail: H.Zhang@uva.nl

Y. Liu
Institute of Chemistry and Biochemistry, Free University of Berlin
14195 Berlin (Germany)

Dr. X. Zhu
School of Physical Science and Technology, Shanghai Tech University
Shanghai 201210 (China)

Introduction

Photothermal-based synergistic therapy enables highly precise treatment of tumors.[1] Among these, photothermal chemotherapy has shown great potential, due to its high efficacy and good complementarity. With optimal laser irradiation, local hyperthermia and drug release can be induced simultaneously, thereby concomitantly activating two therapeutic approaches, which is not only recipient friendly, but also promotes a synergistic effect.[2] Our recently introduced tumor microenvironment response and temperature sensing strategies have further improved the therapeutic precision, by providing customized irradiation prescriptions for each individual case.[3] However, unlike the single tumor-bearing model typically used in research, real cancer cases often show multiple tumors, especially in subcutaneous orthotopic cancers (e.g., breast cancer and fibrosarcoma et al.).[4] Therefore, there is a strong need to realize multi-tumor ablation in vivo, before translating it into real biomedical practice.

One of the major barriers to multi-tumor treatment is the uncertainty of the therapeutic effect between different tumors. Due to individual biological and physiological differences, tumors show varying resistance to drugs and hyperthermia, making it improbable that multiple tumors can be ablated with a single prescription.[5] On the one hand, some tumors would not be effectively ablated with an overall low drug dose and temperature. On the other hand, a high overall prescription would lead to overtherapy, which has been shown be detrimental to patient health. Thus, an individually customized prescription would be preferable for the treatment of multi-tumor cases, to ensure both efficacy and safety. Reduced glutathione (GSH) was found to be a typical indicator in the microenvironment of orthotopic breast tumors, which can vary at different development stages,[6] and has also been linked to multi-drug resistance and self-protection mechanisms in acute stimulation.[7] If the GSH in different tumors could be eliminated to a similar level by a nanocomposite, while the irradiation prescription could be customized based on the nanocomposites′ signal from individual tumors, it would be possible to ablate multiple tumors simultaneously with both, high efficacy and low side effects. Due to their unique optical properties and good biocompatibility, lanthanide-based nanocomposites are widely applied in many bio-applications.[8] Our recent advances in multi-channel strategy have further excavated their potential to orthogonally operate multiple functions in independent signal channels.[9] Therefore, the lanthanide-

based multi-channel nanocomposites could be outstanding candidates to realize the elimination of GSH and customized tumor treatment.

Herein, a strategy for tailored synergistic ablation of multiple tumors is proposed, targeting the intratumoral GSH difference between different tumors in an individual. It is based on a rationally designed silicomolybdate-functionalized $NaLuF_4$:Nd@$NaLuF_4$@$mSiO_2$ nanocomposite, loaded with the model chemotherapeutic drug doxorubicin. This nanocomposite can react with GSH in the acidic tumor microenvironment, thereby activating the ratiometric fluorescence and photothermal channels. The fluorescence ratio allows the evaluation of near-infrared (NIR) absorbance in different tumors with different GSH concentrations, which helps the operators to create a customized irradiation prescription for each individual tumor. As a result, the different intratumoral GSH levels are reduced to similarly low levels by the nanocomposites, while a defined temperature and drug release can be achieved for effective ablation of all tumors at a similar rate. Finally, we successfully applied this strategy in vivo by using a mouse model, bearing two orthotopic breast tumors with different intratumoral GSH levels. Together with our custom-designed therapeutic laser system, a precise, non-uniform whole-body irradiation treatment is possible.

Results and Discussion

Preparation of Multi-Channel Nanocomposite

The multi-channel nanocomposite was designed and prepared as a core-multishell structure (Figure 1A). The uniform core-shell $NaLuF_4$:Nd@$NaLuF_4$ nanophosphor was synthesized by the typical solvothermal method (Figure S1), coated with mesoporous SiO_2 (Ln-mSi) and afterwards modified with silicomolybdenate (Ln-mSiMo).

The obtained $NaLuF_4$:Nd@$NaLuF_4$@$mSiO_2$-$SiMo^{VI}$ (Ln-mSiMo) can be homogeneously dispersed in phosphate-buffered saline (PBS) with a medium yellow appearance, while the transmission electron microscopy (TEM) image showed that the nanocomposites were uniform nanoparticles, coated with a low contrast shell at the periphery (Figure 1B). High-resolution TEM confirmed that the nanocomposites were composed of a highly crystallized lanthanide core and an amorphous shell of $mSiO_2$ and SiMo (Figure 1C), which was supported by powder X-ray diffraction (Figure S2A). Furthermore, the elemental mapping profile by energy-dispersive X-ray analysis showed the distribution of Lu, Si, and Mo in the nanocomposite. It suggests that the Mo^{VI} can be firmly modified and well distributed on the surface of mesoporous SiO_2 (Figure 1D), which is in accordance with the energy-dispersive X-ray spectrum (Figure S2B). The mesoporous structure of Ln-mSiMo was identified by the N_2 absorption-desorption isotherms (Figure 1E), which show a high Brunauer–Emmett–Teller surface area ($45.05 \pm 1.08\ m^2 g^{-1}$) and a large Barrett–Joyner–Halenda pore volume ($0.18 \pm 0.01\ mL g^{-1}$). Attributed to the f-f electronic transition of Nd^{3+} dopant, the nanocomposites exhibit multiple NIR fluorescence emission peaks under 808 nm excitation, including two in the first NIR window 870 nm ($^4F_{3/2} \rightarrow {}^4I_{9/2}$, NIR I) and second NIR window 1060 nm ($^4F_{3/2} \rightarrow {}^4I_{11/2}$, NIR II), respectively (Figure 1F). As evidence of their redox properties, square-wave voltammetry results suggest that the Mo^{VI} on the Ln-mSiMo surface can be partially reduced at 0.225 V and 0.327 V. This can be attributed to the two-step electrons transfer within SiMo (Figure 1G). As a result, the Ln-

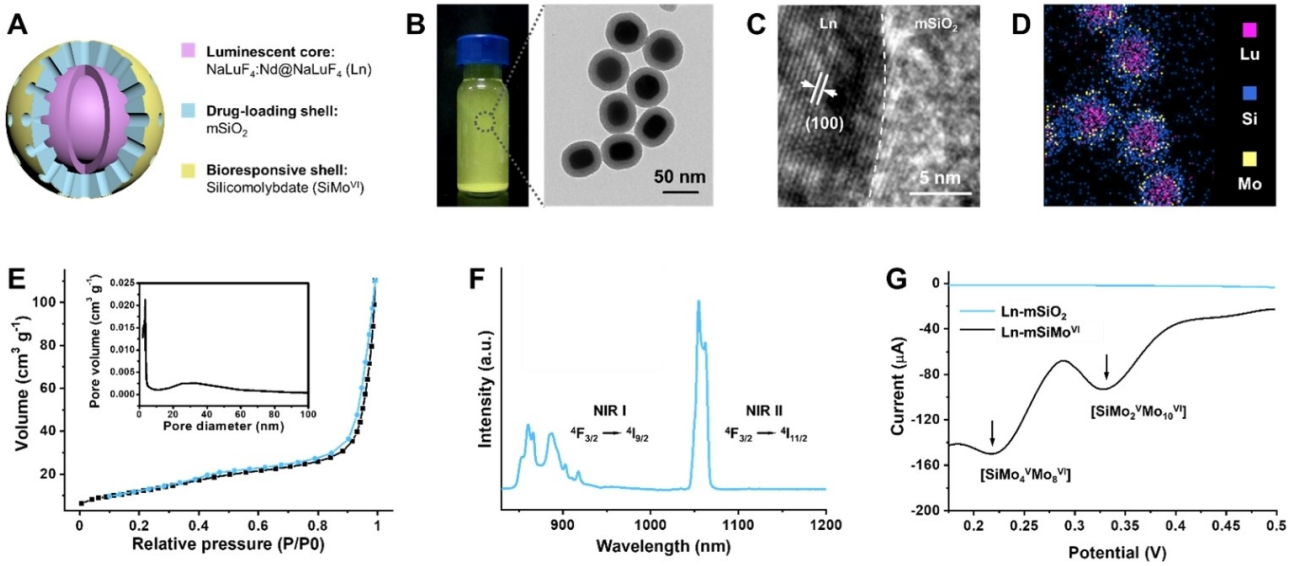

Figure 1. Construction and characterization of Ln-mSiMo. (A) Schematic presentation of as-designed core-multishell Ln-mSiMo. (B) Photograph of as-prepared Ln-mSiMo in PBS (left) and TEM image of Ln-mSiMo (right). High-resolution TEM image (C), energy-dispersive X-ray analysis elemental mapping profile (D), N_2 absorption-desorption isotherms (E), NIR fluorescence spectrum (F), and square-wave voltammetry curve (G) of Ln-mSiMo. Pore size distribution of Ln-mSiMo were inserted in E.

mSiMo can be partially reduced and it contains a mixed valence state of Mo^{V} and Mo^{VI}. Concluding, the redox-responsive fluorescent nanocomposites with mesoporous structure were successfully prepared as defined by design.

Dual Optical Channels Activated by GSH

As a typical reducing agent and characteristic intratumoural indicator, GSH was utilized as a redox target to activate the optical channels of Ln-mSiMo in situ. In the acidic environment containing GSH, Ln-mSiMo is reduced, oxidizing GSH to oxidized glutathione (GSSG). Quantification of residual GSH showed that more than 90 % of GSH was oxidized in the studied GSH concentration range of 100–900 μM (Figure S3). Upon its reduction, Ln-mSiMo acquired a localized surface plasmon resonance peak in the NIR region, originating from the intervalence charge transfer between Mo^{V} and Mo^{VI}. This can quench the NIR fluorescence of Ln-mSiMo through the inner filter effect and generate heat under 808 nm irradiation. Notably, as the GSH level can vary significantly between tumours (from 100 to 900 μM), the Ln-mSiMo would show different NIR absorbance in different tumours (Figure 2A),[10] as indicated by the NIR II/NIR I fluorescence ratio (Figure 2B) and would generate different amounts of heat under irradiation (Figure S4). Therefore, by determining the NIR II/NIR I fluorescence ratio, it would be practical to evaluate the NIR absorbance and predict the heat generation, further reducing the influence of unequal GSH levels on the therapeutic effect on different tumours.

According to previous findings, the eigen temperature (E.T.) of nanocomposites mainly contributed to the photothermal ablation and drug release.[11] Therefore, the E.T. under irradiation was studied by using the thermosensitive fluorescence of Nd^{3+} dopant (Figure S5). It was found that the E.T. of Ln-mSiMo, reduced by the intratumoural GSH level, could reach the therapeutic temperature at the optimal laser density and irradiation time, while those reduced by the GSH level in normal tissues (≈25 μM) did not, indicating that the Ln-mSiMo could be used for selective tumour ablation (Figure 2C).

With a mesoporous structure, the Ln-mSiMo can load chemotherapeutic drugs (e.g., doxorubicin, *abbr.* Ln-mSiMo-dox) into its pores and release them by diffusion upon an external trigger (Figure S6). To clarify the process of E.T.-triggered drug release, the possible temperature distribution around a pore of a Ln-mSiMo was simulated by using a single-particle model that was established by the finite element method (FEM). According to the thermal conduction simulation, when the SiMo layer generates heat upon irradiation, both the $mSiO_2$ and the surrounding water are heated up simultaneously (Figure 2D). During thermal

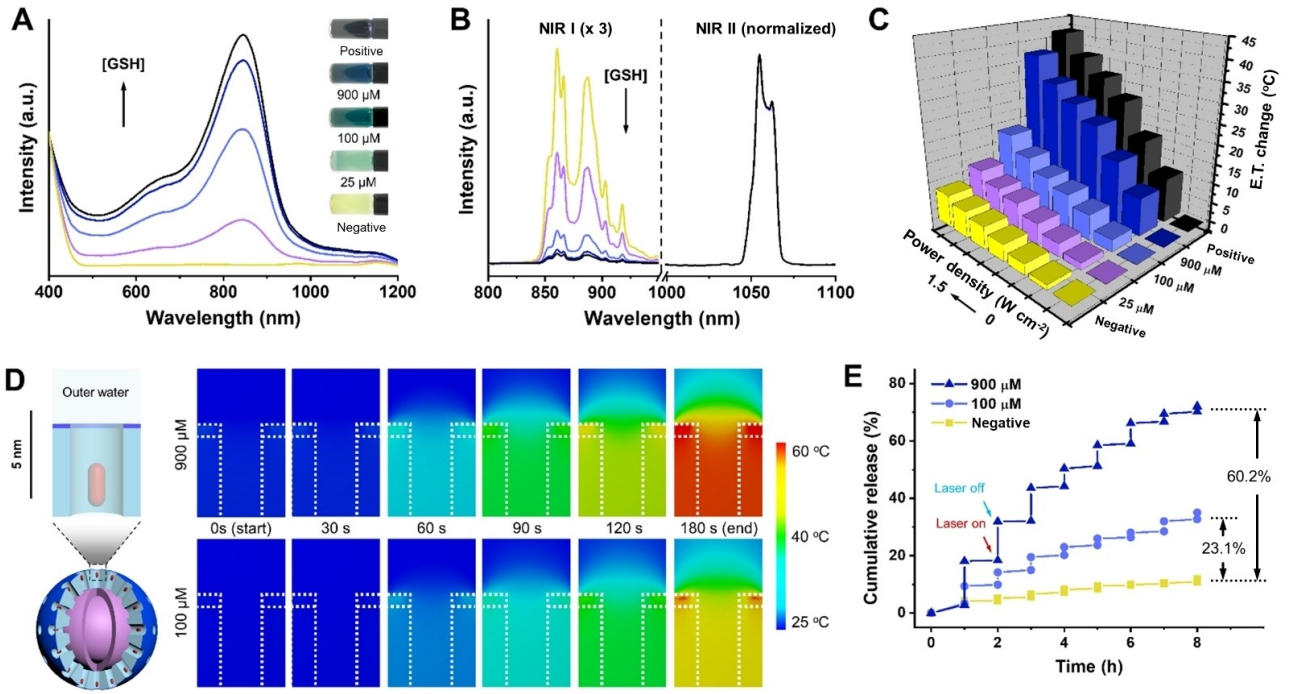

Figure 2. GSH-activated fluorescence and photothermal effect. Absorbance spectra (A) and fluorescence spectra (B) of Ln-mSiMo at different concentrations of GSH. The GSH concentration was 0, 25 μM, 100 μM, 900 μM, and 1 mM, increasing in the direction of the arrow. (C) Eigen temperature (E.T.) change of Ln-mSiMo at different concentrations of GSH as a function of laser power density. The studied GSH concentration range covers the typical GSH levels in normal tissue (25 μM), in low-GSH tumor (100 μM), and in high-GSH tumor (900 μM). The Ln-mSiMo in PBS (negative) and reduced Ln-mSiMo (positive) were used as negative and positive control, respectively. (D) FEM simulation of the heat evolution process induced by the photothermal effect on a single Ln-mSiMo-dox particle in intratumoral GSH levels (100 μM and 900 μM) at different time points. (E) Release profile of doxorubicin in saline buffer at acidic conditions (pH = 5.5) in the absence and presence of 808 nm NIR laser (0.75 W cm^{-2}, 3 min) within 8 hours.

equilibrium, their thermal diffusivity (α) is a critical factor, which can be calculated using the following equation:

$$\alpha = \frac{\lambda}{\rho c}$$

where λ is the thermal conductivity ($W m^{-1} K^{-1}$), ρ is the density ($kg m^{-3}$) and c is the specific heat capacity ($J kg^{-1} K^{-1}$). According to the CAS standard parameters, the α of amorphous $mSiO_2$ ($6.98 \times 10^{-7} m^2 s^{-1}$) is almost six times higher than that of water ($1.19 \times 10^{-7} m^2 s^{-1}$), which suggests that the $mSiO_2$ would reach thermal equilibrium much faster than the water outside, further heating up the water in the pores and generating a temperature gradient. Therefore, increasing the E.T. accelerated the heat convection and thus promoted the drug release (Figure 2E).

The above results demonstrated that the Ln-mSiMo can respond to the intratumoural concentration of GSH, possess GSH concentration-dependent ratiometric fluorescence and increase the E.T. upon irradiation. The ratiometric fluorescence was linked to the NIR absorbance, which was the critical factor that would influence the photo-induced hyperthermia and drug release for tumour ablation.

Prediction of Synergistic Therapeutic Effect

To reveal the relationship between the different parameters, the calibration diagrams of irradiation prescription *vs* E.T. or drug release amount were first established. According to the intratumoral GSH range, nine orthogonal case models of Ln-mSiMo-dox were reduced by different concentrations of GSH and implanted in tissue phantoms, respectively. The NIR II/NIR I fluorescence ratios of reduced Ln-mSiMo-dox in different cases were recorded, while their E.T. and drug release amounts were determined as a function of laser power density and irradiation time. It was observed that the Ln-mSiMo-dox reduced by higher GSH concentrations exhibited larger NIR II/NIR I fluorescence ratios than those reduced by lower GSH concentrations, contributing to the fluorescence quenching effect of GSH-reduced SiMo (Figure 3A). Notably, at various NIR II/NIR I fluorescence ratios, the reduced Ln-mSiMo-dox could reach similar E.T. and release similar amounts of the chemotherapeutic drug, simply by using different laser power densities and irradiation times (Figure 3B and 3C). These results suggest that by knowing the fluorescence ratio, a desired E.T. and drug release can be achieved for the treatment under pre-established irradiation prescriptions.

Further efforts were made to confirm the practicability in tumour cells. Calibration diagrams were established between irradiation prescriptions and tumour cell viability, by using the nine similar models as in vitro tests. As the NIR II/NIR I fluorescence ratio increased, more tumour cells died at the same irradiation prescription, caused by the generation of more heat and the release of more chemotherapeutic drugs (Figure 4A). Notably, the cell killing was similar even though the E.T. and the released drug amount were different in the same GSH setting. This confirmed the synergistic effect of photothermal therapy and chemotherapy. Next, a double-blind experiment was performed by using tumour cells with random GSH concentration (Figure 4B). All the cell groups were incubated with the Ln-mSiMo-dox before the fluorescence ratio was tested. Subsequently, the irradiation prescription for each individual group was established according to the calibration diagrams, ensuring that all treatments could be terminated at a similar time point, and the customized synergistic therapy was performed. Of all 100 studied groups, 96 groups of cells were effectively eliminated, indicating that our customized

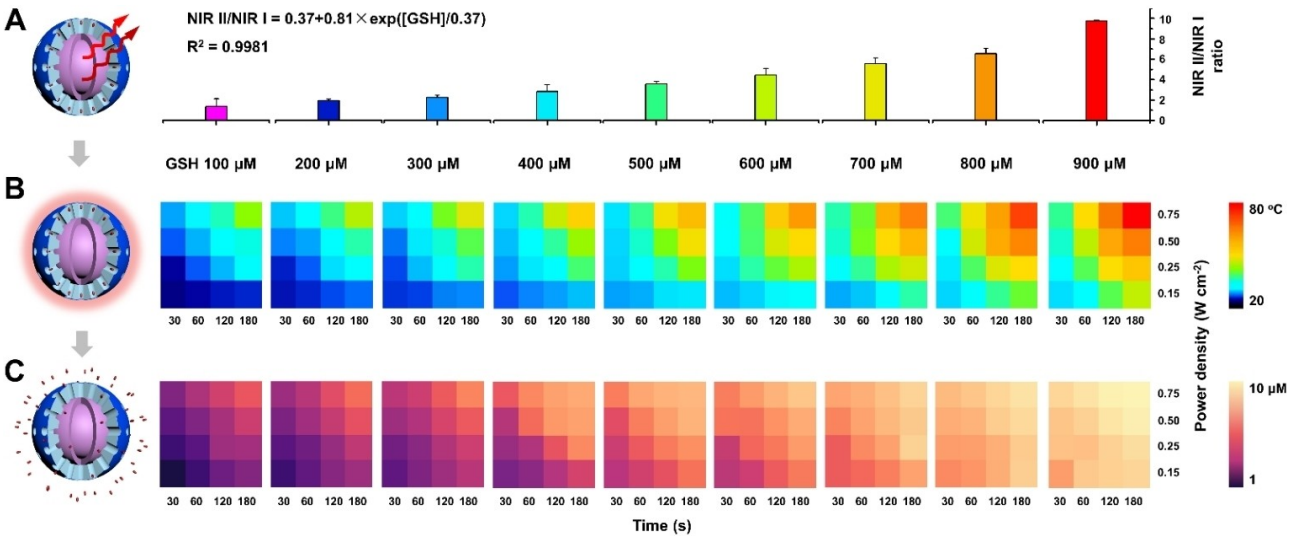

Figure 3. Relationship between fluorescence ratio, E.T. generation, and drug release amount. NIR II/NIR I fluorescence ratio (A), E.T. (B), and drug release amount (C) of Ln-mSiMo-dox in the presence of different intratumoral GSH levels. The E.T. and drug release amount were collected as a function of laser power density and irradiation time, which was considered as two parameters in the irradiation prescription. Data are represented as mean ± SD ($n = 3$).

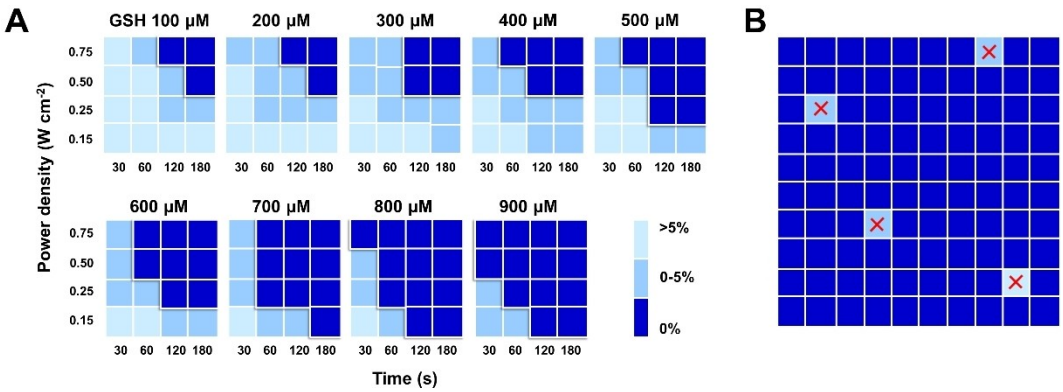

Figure 4. Effective customized synergistic treatment of tumor cells by fluorescence prediction. (A) Viability of tumor cells incubated with Ln-mSiMo-dox in the presence of different intratumoral GSH levels as a function of laser power density and irradiation time. Tumor cell groups with viability of 0% were highlighted. (B) Cell viability in 100 random samples after receiving customized irradiation prescription. Tumor cell groups with viability higher than 0% were marked by a red cross.

prescription had an effectiveness of more than 90%, which was worth testing in vivo (Figure 4C). As a result, it was practical to treat different tumours simultaneously with a similar therapeutic effect by varying the irradiation prescription, which could be customized based on the determined fluorescence ratio.

Highly Efficacious Customized Synergistic Therapy

To evaluate the synergistic therapeutic efficacy of customized irradiation prescription, random mice bearing two orthotopic breast tumors (dual tumor model) were studied. For this purpose, a ring-shaped laser array containing 8 laser fibers was constructed with a stage, which could cover the whole body of a mouse and generate a non-uniform irradiation according to the customized prescriptions for individual tumors (Figure 5A). To demonstrate the feasibility, GSH-modulated mice were obtained by a mature L-buthionine-sulfoximine method (Figure S7), which had one tumor with normal GSH level (GSH (H)) and another one with decreased (GSH (L)).[12] The fluorescence images of the mice showed that the GSH (H) tumor possessed a higher NIR II/NIR I fluorescence ratio than the GSH (L) tumor (Figure 5B), which allowed the establishment of customized prescriptions in reference to the calibration diagrams shown in Figure 4A. Fluorescence images of harvested organs showed accumulation of Ln-mSiMo in both tumors, indicating their applicability for synergistic treatment (Figure S8). Upon administration of the nanocomposite (Ln-mSiMo (+)), the temperature of tumors was increased under laser irradiation, while no change was observed for the ones without administration (Ln-mSiMo (−)), which illustrated the selective heat generation by Ln-mSiMo in tumors (Figure 5C). Compared to the mice receiving dox-free Ln-mSiMo with laser irradiation (photothermal therapy group, $\Delta V = -40.88 \pm 9.10\ mm^3$) and Ln-mSiMo-dox without laser irradiation (chemotherapy group, $\Delta V = -29.08 \pm 10.49\ mm^3$), those receiving Ln-mSiMo-dox with laser irradiation (synergistic therapy group, $\Delta V = -52.41 \pm 8.43\ mm^3$) showed a much better tumor ablation effect after 12-days treatment (Figure S9). However, under normal uniform laser irradiation, the temperature of different tumors increased unequally, caused by the low NIR absorbance in response to the decreased intratumoral GSH level, resulting in different therapeutic efficacies (Figure 5D). In contrast, under non-uniform laser irradiation by customized prescription, both GSH (H) and GSH (L) tumors could reach similar temperatures, which contributed to the similarly effective ablation of both tumors. Therefore, since the Ln-mSiMo is biocompatible (Figure S10), the photothermal-chemo synergistic ablation of multiple tumors was realized in vivo by using customized irradiation prescription.

For validation, a double-blind customized tumor therapy was performed. After performing ratiometric fluorescence imaging and establishing irradiation prescription, the dual-tumor-bearing mice received customized synergistic therapy under non-uniform irradiation (Figure 6A). The changes in tumor size, body weight, and viability were collected to evaluate the therapeutic efficacy and safety. It was observed that the sizes of both tumors in mice receiving customized irradiation prescription decreased after 12-days treatment ($V_{max} - V_{min} = 3.7\ mm^3$, Figure 6B, Table S1), which was similar to the therapeutic effect of those receiving uniform high laser irradiation (2.5 mm^3, Table S2). In contrast, those mice receiving uniform low laser irradiation, obviously showed different changes in tumor size due to the varying therapeutic effect (16.3 mm^3, Table S3). However, when taking viability into consideration, customized irradiation (100%) and uniform low irradiation prescription (80%) worked better on mice than the uniform high irradiation prescription (50%), which was a result of less side effects from overdose of chemotherapeutic drug and hyperthermia injury (Figure 6C). The change in body weight also supported this explanation, as the mice receiving uniform high irradiation prescription, lost weight over time (-1.6 ± 2.3 g), even though the tumors were effectively ablated (Figure 6D). In contrast, the mice receiving customized irradiation recovered better (5.1 ± 2.6 g). For further comparison, the widely-

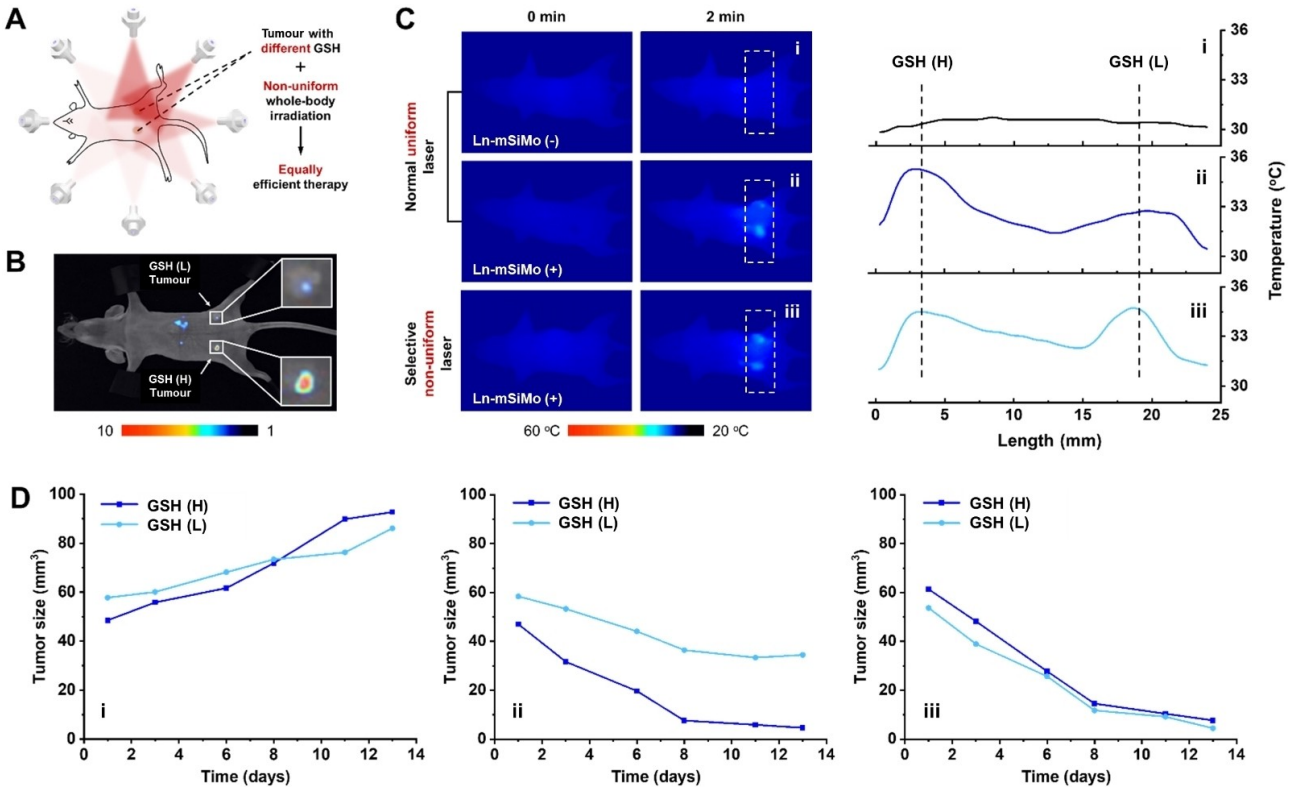

Figure 5. Similar heat generation in different tumors by non-uniform irradiation. (A) Schematic presentation of the non-uniform whole-body irradiation by using an accessional therapeutic instrumental system. (B) NIR II/NIR I ratiometric fluorescence imaging of a mouse bearing a dual orthotopic breast tumor with different GSH levels. Thermal imaging and temperature distribution (C) and change of tumor size (D) of the mice bearing a dual orthotopic breast tumor with different GSH levels receiving different treatment, including (i) PBS injection + uniform irradiation, (ii) Ln-mSiMo-dox injection + uniform irradiation, and (iii) Ln-mSiMo-dox injection + customized non-uniform irradiation. The customized non-uniform irradiation prescription was established based on the ratiometric fluorescence imaging result of the mouse.

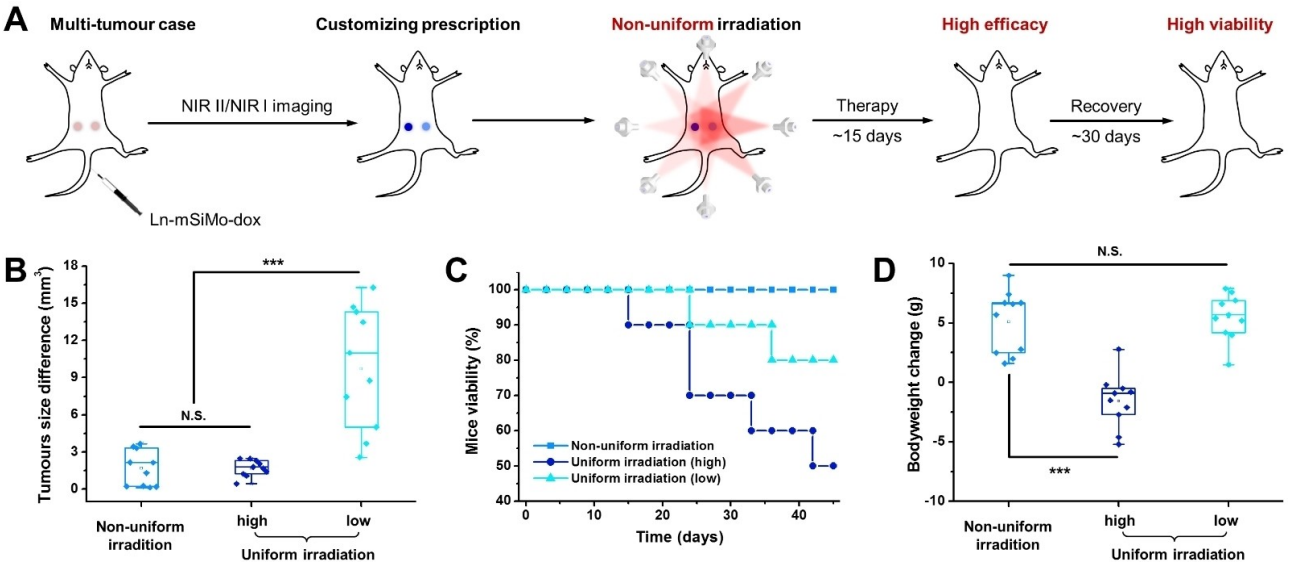

Figure 6. Effective multi-tumor ablation in vivo with fluorescence prediction. (A) Schematic presentation of treating multi-tumor cases under non-uniform whole-body irradiation based on customized irradiation prescription. Difference in tumor size (B), viability (C), and bodyweight change (D) of mice after 12 days receiving non-uniform irradiation according to the customized prescription ($n = 10$). Mice receiving uniform high and low irradiation were used for comparison, respectively.

used non-GSH-responsive photothermal conversion agent, indocyanine green, was modified on the Ln-mSi (Ln-mSi-ICG, Figure S11). Without knowledge of intratumoral information, only uniform irradiation prescription could be applied to the mice, receiving Ln-mSi-ICG-dox administration, resulting in worse therapeutic efficacy than those receiving Ln-mSiMo-dox and customized non-uniform irradiation prescription (Figure S12). Therefore, it was reasonable to conclude that multiple orthotopic breast tumors could be ablated simultaneously and similarly, by using the as-constructed nanocomposite and customized irradiation prescription with outstanding efficacy and safety.

Conclusion

A $NaLuF_4$:Nd@$NaLuF_4$@$mSiO_2$–$SiMo^{VI}$ nanocomposite with fluorescent and photothermal channels was prepared for customized synergistic treatment of an orthotopic breast cancer model case with multiple tumors. In an acidic tumor microenvironment, the nanocomposite can react with the intratumoral GSH, eliminating $>90\,\%$ of GSH to a similarly low level of $<50\,\mu M$. Meanwhile, the two optical channels are simultaneously activated, enabling diagnostic and therapeutic functions, respectively. Through the inner filter effect between the lanthanide core and reduced SiMo, the fluorescence of the nanocomposite centered at 870 nm (NIR I) and 1060 nm (NIR II) could indicate the change of its own NIR absorbance in the tumor microenvironment. This provided sufficient information to evaluate their photothermal properties and thereby to predict the photothermal therapeutic effect under different irradiation prescriptions. According to the simulation of thermal distribution, the photo-induced hyperthermia could also generate a temperature gradient at the nanoscale, which promoted drug release and triggered chemotherapy. Therefore, it was practical to control and predict the efficacy of both photothermal therapy and chemotherapy by a customized irradiation prescription.

To perform different irradiation prescriptions on different tumors in one case, an 808 nm ring-shaped laser array was constructed and attached to a stage to generate a light field with non-uniform power density (Figure S13). Based on this therapeutic platform, the photo-induced synergistic therapy could be realized by adjusting the laser power density and irradiation time according to the pre-established prescription.

After receiving the customized irradiation, the two orthotopic breast tumors in a small animal case were simultaneously ablated with similarly high efficacy (V_{max}–$V_{min}=3.7\ mm^3$ for the customized therapy group *vs* $16.3\ mm^3$ for the non-customized low irradiation group) and less side effects (100 % viability and 5.1 ± 2.6 g change in body weight for the customized therapy group *vs* 50 % viability and -1.6 ± 2.3 g change in body weight for the non-customized high irradiation group). In addition, our nanocomposite was also superior to the widely used indocyanine green-modified nanocomposite ($5.4\ mm^3$, 80 % viability, and 4.2 ± 1.8 g change in body weight with low irradiation prescription).

This work proposed a strategy for the treatment of multi-tumor cases by using customized irradiation prescriptions, aimed at individual differences between tumors. In other words, multiple tumors can be ablated simultaneously by matching their intratumoral difference by adjusting the laser irradiation. In summary, this customized therapeutic option could be applied in the pharmaceutical and medical industry, when facing the challenge of multi-tumor cases. The results of this work indicate the possibility of treating multiple orthotopic tumors with equal efficacy and highlight the adaptability of the multi-channel nanomaterials in practical medical situations. Still, there are several issues that need to be addressed in the future. First, the structure of the Ln-mSiMo-dox is rather complex, which should be simplified to improve the production process and yield. In addition, bioavailability of the nanocomposite should be improved by adjusting the morphology, surface engineering, and/or conjugation with targeting ligands. Finally, metabolism and clearance pathways of the nanocomposite should be carefully studied. Therefore, further investigation on this nanocomposite for customized synergistic treatment is needed.

Author Contributions

Y.L. conceived the project, analyzed the data and wrote the original manuscript. F.F.L., J.Z., and H.Z. mainly supervised the project, while F.F.L., J.Z., H.Z., X.Z., Z.W., and F.G.M. acquired the financial support. Y.L. and X.Z. designed the methodology and established the model for study. Y.L. performed the experiments in cooperation with Z.W., K.W., JF.Z. and X.Z. F.F.L., J.Z., H.Z. and F.G.M. provided main resource support. Y.L., X.Z., F.F.L., J.Z., and H.Z. decided on the visualization and data presentation. All authors contributed to the review and editing of manuscript.

Acknowledgements

The authors thank the financial support from the German Federal Ministry of Education and Research (BMBF, 13XP5050A, F.F.L.), the Max-Planck-Fraunhofer collaboration project (Glyco3Display, F.F.L.), the Max Planck Society, EU H2020-MSCA-RISE-2017 Action program (CANCER, 777682, H.Z.), National Natural Science Foundation of China (92159103, J.Z.; 82001945, X.Z.), Shanghai Pujiang Program (20PJ1410700, X.Z.), NWO Sector Plan for Physics and Chemistry (F.G.M.), and China Scholarship Council scholarship (202008110184, Z.W.). Y.L. personally thanks Prof. Fuyou Li from Fudan University and Prof. Zhanfang Ma from Capital Normal University for crucial support and guidance. Open Access funding enabled and organized by Projekt DEAL.

Conflict of Interest

The authors declare no conflict of interest.

Data Availability Statement

The data that support the findings of this study are available in the supplementary material of this article.

Keywords: Drug Release · Fluorescent Probes · Lanthanide-Doped Nanoparticles · Synergistic Therapy · Temperature Sensing

[1] a) Z. J. Xie, T. J. Fan, J. An, W. Choi, Y. H. Duo, Y. Q. Ge, B. Zhang, G. H. Nie, N. Xie, T. T. Zheng, Y. Chen, H. Zhang, J. S. Kim, *Chem. Soc. Rev.* **2020**, *49*, 8065–8087; b) C. Liang, L. G. Xu, G. S. Song, Z. Liu, *Chem. Soc. Rev.* **2016**, *45*, 6250–6269.

[2] a) M. Craig, A. L. Jenner, B. Namgung, L. P. Lee, A. Goldman, *Chem. Rev.* **2021**, *121*, 3352–3389; b) W. P. Fan, B. Yung, P. Huang, X. Y. Chen, *Chem. Rev.* **2017**, *117*, 13566–13638.

[3] Y. X. Liu, X. J. Zhu, Z. Wei, W. Feng, L. Y. Li, L. Y. Ma, F. Y. Li, J. Zhou, *Adv. Mater.* **2021**, *33*, 2008615.

[4] a) R. Karki, S. M. Man, T. D. Kanneganti, *Cancer Immunol. Res.* **2017**, *5*, 94–99; b) G. M. Allen, W. A. Lim, *Nat. Rev. Cancer* **2022**, *22*, 693–702.

[5] M. Labrie, J. S. Brugge, G. B. Mills, I. K. Zervantonakis, *Nat. Rev. Cancer* **2022**, *22*, 323–339.

[6] a) C. R. Corso, A. Acco, *Crit. Rev. Oncol. Hematol.* **2018**, *128*, 43–57; b) F. Gong, N. L. Yang, X. W. Wang, Q. Zhao, Q. Chen, Z. Liu, L. Cheng, *Nano Today* **2020**, *32*, 100851; c) S. C. Nunes, J. Serpa, *Int. J. Mol. Sci.* **2018**, *19*, 1882.

[7] a) N. Traverso, R. Ricciarelli, M. Nitti, B. Marengo, A. L. Furfaro, M. A. Pronzato, U. M. Marinari, C. Domenicotti, *Oxid. Med. Cell. Longevity* **2013**, *2013*, 972913; b) D. S. Backos, C. C. Franklin, P. Reigan, *Biochem. Pharmacol.* **2012**, *83*, 1005–1012; c) Y. X. Xiong, C. Xiao, Z. F. Li, X. L. Yang, *Chem. Soc. Rev.* **2021**, *50*, 6013–6041.

[8] a) F. Auzel, *Chem. Rev.* **2004**, *104*, 139–173; b) J. Zhou, Z. Liu, F. Y. Li, *Chem. Soc. Rev.* **2012**, *41*, 1323–1349; c) A. Gnach, T. Lipinski, A. Bednarkiewicz, J. Rybka, J. A. Capobianco, *Chem. Soc. Rev.* **2015**, *44*, 1561–1584; d) W. Zheng, P. Huang, D. T. Tu, E. Ma, H. M. Zhu, X. Y. Chen, *Chem. Soc. Rev.* **2015**, *44*, 1379–1415; e) J. T. Xu, A. Gulzar, P. P. Yang, H. T. Bi, D. Yang, S. L. Gai, F. He, J. Lin, B. G. Xing, D. Y. Jin, *Coord. Chem. Rev.* **2019**, *381*, 104–134; f) A. H. All, X. Zeng, D. B. L. Teh, Z. G. Yi, A. Prasad, T. Ishizuka, N. Thakor, Y. Hiromu, X. G. Liu, *Adv. Mater.* **2019**, *31*, 1803474; g) Y. D. Ding, X. Hong, Y. C. Liu, H. Zhang, *Curr. Pharm. Des.* **2019**, *25*, 2007–2015; h) R. C. Lv, M. Raab, Y. X. Wang, J. Tian, J. Lin, P. N. Prasad, *Coord. Chem. Rev.* **2022**, *460*, 214486.

[9] a) Y. X. Liu, Z. Wei, X. Q. Liao, J. Zhou, *Acc. Mater. Res.* **2020**, *1*, 225–235; b) Y. X. Liu, Z. Wei, J. Zhou, Z. F. Ma, *Nat. Commun.* **2019**, *10*, 5361; c) Z. Wei, T. Q. Cao, L. Y. Li, X. J. Zhu, J. Zhou, Y. X. Liu, *Chem. Commun.* **2022**, *58*, 9642–9645.

[10] M. J. Allalunisturner, F. Y. F. Lee, D. W. Siemann, *Cancer Res.* **1988**, *48*, 3657–3660.

[11] a) X. J. Zhu, J. C. Li, X. C. Qiu, Y. Liu, W. Feng, F. Y. Li, *Nat. Commun.* **2018**, *9*, 2176; b) X. J. Zhu, W. Feng, J. Chang, Y. W. Tan, J. C. Li, M. Chen, Y. Sun, F. Y. Li, *Nat. Commun.* **2016**, *7*, 10437.

[12] a) T. Nakamura, H. Matsushita, F. Sugihara, Y. Yoshioka, S. Mizukami, K. Kikuchi, *Angew. Chem. Int. Ed.* **2015**, *54*, 1007–1010; b) M. J. Allalunisturner, R. S. Day, J. D. S. McKean, K. C. Petruk, P. B. R. Allen, K. E. Aronyk, B. K. A. Weir, D. Huyserwierenga, D. S. Fulton, R. C. Urtasun, *J. Neuro-Oncol.* **1991**, *11*, 157–164.

Manuscript received: March 10, 2023
Accepted manuscript online: April 26, 2023
Version of record online: May 10, 2023